JCI The Journal of Clinical Investigation

Breast cancer cell-derived microRNA-155 suppresses tumor progression via enhancing immune cell recruitment and anti-tumor function

Junfeng Wang, … , Guoshuai Cai, Daping Fan

J Clin Invest. 2022. https://doi.org/10.1172/JCI157248.

Research In-Press Preview Immunology

Graphical abstract

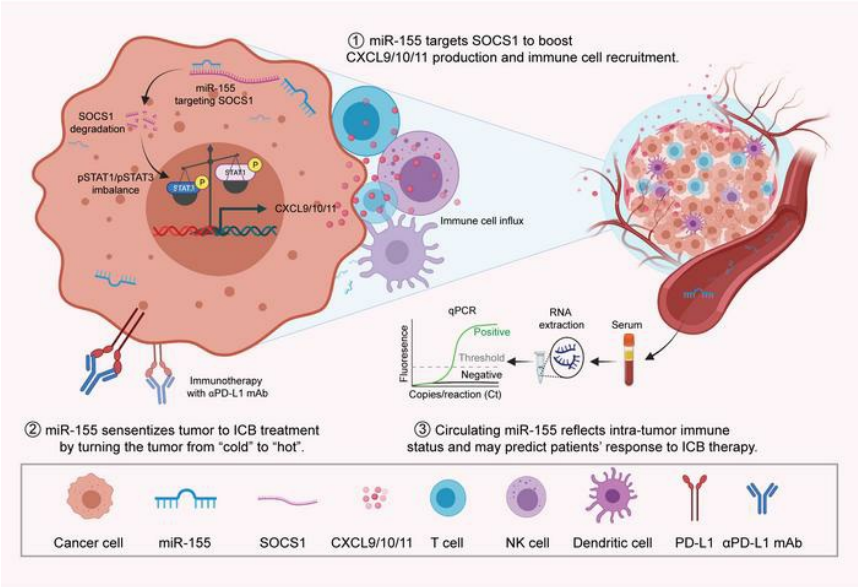

Breast cancer cell-derived microRNA-155 suppresses tumor progression via enhancing immune cell recruitment and anti-tumor function

Junfeng Wang[1]*, Quanyi Wang[1,2], Yinan Guan[3], Yulu Sun[3], Xiaozhi Wang[1,4], Kaylie Lively[1], Yuzhen Wang[1], Ming Luo[5], Julian A. Kim[6], E. Angela Murphy[7], Yongzhong Yao[3]*, Guoshuai Cai[8], Daping Fan[1]*

[1]Department of Cell Biology and Anatomy, University of South Carolina School of Medicine, Columbia, South Carolina, USA

[2]Department of Life science and Technology, China Pharmaceutical University, Nanjing, China

[3]Department of General Surgery, Nanjing Drum Tower Hospital, the Affiliated Hospital of Nanjing University Medical School, Nanjing, China

[4]Department of Cardiology, the First Affiliated Hospital of Nanjing Medical University, Nanjing, China

[5]Department of Chemistry, Georgia State University, Atlanta, Georgia, USA

[6]Prisma Health Surgical Oncology, Department of Surgery, University of South Carolina School of Medicine, Columbia, South Carolina, USA

[7]Department of Pathology, Microbiology and Immunology, University of South Carolina School of Medicine, Columbia, South Carolina, USA

[8]Department of Environmental Health Science, Arnold School of Public Health, University of South Carolina, Columbia, South Carolina, USA

* Correspondence to Junfeng Wang, 6439 Garners Ferry Road, Building 1, C36. Columbia, SC 29209, USA. Tel: +1 (803) 216 3834; Email: junfengwang417@gmail.com;

or Yongzhong Yao, Department of General Surgery, The Affiliated Drum Tower Hospital, Medical School of Nanjing University, No. 321 Zhongshan road, Nanjing, 210008, China. Tel: +86 (25) 8310 6666-220611; Email: loyal1006@hotmail.com; or Daping Fan, 6439 Garners Ferry Road, Building 1, C36. Columbia, SC 29209. Tel: +1 (803) 216 3806; Email: daping.fan@uscmed.sc.edu.

Conflict-of-interest statement

The authors have declared that no conflict of interest exists.

Abstract

Evidence suggests that increased microRNA-155 (miR-155) expression in immune cells enhances anti-tumor immune responses. However, given the reported association of miR-155 to tumorigenesis in various cancers, a debate is provoked on whether miR-155 is oncogenic or tumor suppressive. We aimed to interrogate the impact of tumor miR-155 expression, particularly cancer cell-derived miR-155, on anti-tumor immunity in breast cancer. We performed bioinformatic analysis of human breast cancer databases, murine experiments, and human specimen examination. We revealed that higher tumor miR-155 levels correlate with a favorable anti-tumor immune profile and better patient outcomes. Murine experiments demonstrated that miR-155 overexpression in breast cancer cells enhanced T cell influx, delayed tumor growth, and sensitized the tumors to immune checkpoint blockade (ICB) therapy. Mechanistically, miR-155 overexpression in breast cancer cells upregulated their CXCL9/10/11 production, which was mediated by SOCS1 inhibition and increased pSTAT1/pSTAT3 ratio. We further found that serum miR-155 levels in breast cancer patients correlate with tumor miR-155 levels and tumor immune status. Our findings suggest that high serum and tumor miR-155 levels may be a favorable prognostic marker for breast cancer patients, and therapeutic elevation of miR-155 in breast tumors may improve the efficacy of ICB therapy via remodeling the anti-tumor immune landscape.

Introduction

miR-155 was first identified as an oncomiR; it was found to promote carcinogenesis and disease progression of various hematological malignancies and solid tumors (1, 2). It is upregulated in cancers such as breast, liver, lung, pancreatic, and prostate cancers (3-6). Nevertheless, some reports have shown that miR-155 upregulation in tumors is associated with improved overall survival of patients with several types of cancer including breast cancer, colon cancer, and melanoma (7-9). To account for this discrepancy, we and others have shown that miR-155 may play a central role in innate and adaptive immune responses (10-16). We reported that miR-155 deficiency in macrophages and myeloid-derived suppressor cells (MDSCs) promotes tumor growth by exaggerating the immunosuppressive functions of these cells (12, 13). We also showed that miR-155 deficiency impairs dendritic cell (DC) maturation, cytokine secretion, migration toward tumor draining lymph nodes, and their ability to activate T cells, whereas miR-155 overexpression enhances these activities (14). Furthermore, using miR-155 overexpressing DCs, we generated a therapeutic vaccine that resulted in enhanced antitumor immunity against established breast tumors in mice, evidenced by increased intratumor effector T cells, suppressed tumor growth, and drastically reduced lung metastasis (15). miR-155 is also upregulated in activated lymphocytes and involved in T cell and B cell proliferation and maturation (17, 18). Depletion of miR-155 was intrinsically detrimental to the antitumor response of $CD8^+$ cytotoxic T cells (19).

Since miR-155 is expressed in both immune cells and cancer cells in the tumors, an open question is if miR-155 expression in breast tumors in general, and particularly in breast cancer cells, is pro- or anti-tumor. To answer this question, we performed bioinformatic

analyses of human breast cancer databases, murine experiments, and human specimen examinations. We revealed that higher miR-155 levels in breast tumors are associated with a favorable anti-tumor immune infiltration and better patient outcomes, and that miR-155 expressed in breast cancer cells suppressed tumor progression by enhancing the recruitment of anti-tumor immune cells. Furthermore, we observed that miR-155 overexpressing tumors were more sensitive to ICB treatment in a mouse breast cancer model and that serum miR-155 abundance reflected intratumor miR-155 levels as well as the anti-tumor immune status of patients.

Our findings in this study are of great translational and clinical value. Mirroring the immune status of breast tumors, circulating miR-155 levels may be used as a prognostic biomarker of breast cancer patients and as a predictive marker for their responsiveness to immunotherapeutic treatment. Moreover, strategies that enhance miR-155 expression in breast tumors may boost anti-tumor immunity and enhance the efficacy of ICB therapy.

Results

miR-155 expression levels in breast tumors are associated with disease progression

To investigate the association of miR-155 with global gene expression and the clinical outcome of breast cancer patients, we retrieved and analyzed breast cancer data of miRNA-Seq, RNA-Seq, and clinical information from The Cancer Genome Atlas (TCGA) Program (Supplemental Figure 1). After normalization and combination of the raw data, we found that miR-155 expression in human breast tumors was markedly higher than that in adjacent normal tissues (Supplemental Figure 2A). In 99 paired samples, we also observed that miR-155 levels were substantially higher in tumors compared to non-tumor tissues from the same patients (Figure 1A). We confirmed this result by quantitative real-time PCR (qPCR) using freshly resected samples from a small cohort of breast cancer patients (Figure 1B, Supplemental Table 1). Aligning to these findings, we performed a Gene Set Enrichment Analysis (GSEA) and found that miR-155 target genes were less enriched in tumors compared to non-tumor tissues (Figure 1C), consistent with higher miR-155 levels in tumors and the degradation/depletion of miR-155 target genes.

To evaluate how miR-155 levels in tumors were associated with tumor progression, we analyzed relevant clinical information and associated the data with miR-155 expression in tumor tissues of breast cancer patients. The results showed that tumor miR-155 levels were higher in patients at early clinical stages (stage I and II; n = 732) than those at advanced stages (stage III and IV; n = 204) (Figure 1D). In addition, in patients that had lymph node metastasis (N1-N3; n = 520), lower miR-155 levels were observed in their tumor tissues when compared to patients without lymph node involvement (N0; n = 458) (Figure 1E). In

addition, GSEA results revealed that in patients with miR-155 expression levels at upper half (miR-155^{high}, n = 497), gene signatures associated with the downregulation of cancer amplification, metastasis, and relapse were extensively enriched, whereas the opposite was seen in patients with miR-155 expression levels at lower half (miR-155^{low}, n = 498) (Figure 1, F and G).

miR-155 levels in breast cancer tissues correlate with the outcome of patients

Based on the miR-155 expression level in the tumor tissues, we categorized the upper and lower quartiles of patients in TCGA database as miR-155^{high} and miR-155^{low}, with 246 patients in each group. Compared to miR-155^{low} patients, miR-155^{high} patients exhibited an extended survival time (Figure 2A). Multivariate Cox proportional hazards analysis demonstrated that high miR-155 expression in tumors was a protective factor for breast cancer patients (HR = 0.724, P = 0.028) (Supplemental Table 2), suggesting that miR-155 can be used as an independent prognostic factor for breast cancer patients. To confirm this result, we analyzed the relationship between miR-155 or miR-155 host gene (*miR155HG*) expression levels with the overall survival of different cohorts of breast cancer patients. The data of European Genome-Phenome Archive (EGA) cohort showed that patients with higher miR-155 levels had extended survival time, although statistical significance was not reached (P = 0.34) (Supplemental Figure 2B). Notably, the result of meta-analysis based multiple Gene Expression Omnibus (GEO) datasets, which was retrieved from Kaplan-Meier (KM) plotter, supports a positive relationship between *miR155HG* expression levels and the survival rate of breast cancer patients (Figure 2B). To further interrogate the relationship between miR-155 levels and the prognosis of patients with cancers of differing molecular

classifications, we generated KM survival curves of various breast cancer subtypes with different miR-155 expression levels; the results showed that in EGA and GEO cohorts, miR-155 or *miR155HG* expression levels were positively associated with the outcome of breast cancer patients, regardless of molecular subtype, although the association is not statistically significant in the Luminal A and HER2 patients (Figure 2, C and D). By analyzing TCGA patient groups based on the median value of their tumor miR-155 expression levels, we also found a significant association between miR-155 expression levels and overall survival of Luminal B patients; and similar trends were also observed in Basal-like and HER2-type breast cancer patients, although the associations were not statistically significant due to the small sample size (Supplemental Figure 2C).

Collectively, these data suggest that miR-155 expression levels in breast tumors are inversely associated with breast cancer progression and positively correlated with better patient outcome. Based on our recent findings indicating that miR-155 is a central regulator of anti-tumor immunity (12-15), we speculate that patients who have high tumoral miR-155 expression may have enhanced anti-tumor immune responses.

Higher miR-155 expression defines a better anti-tumor immune profile in human breast tumors

To investigate whether high miR-155 expression in tumors was associated with an enhanced anti-tumor immune response, we first analyzed differentially expressed genes (DEGs) between miR-155^{high} and miR-155^{low} tumors from TCGA database. Based on the preset criteria of Log2 fold change $\geq$ 1 and adjusted *P* value < 0.05, 293 out of 12,885 genes were shown to be differentially expressed, including 283 genes that were upregulated and

10 genes that were downregulated in miR-155^{high} tumors (Figure 3A). The DEGs with a Log2 fold change of at least 2.0 (n = 64) are shown in Supplemental Table 3. Functional enrichment of DEGs was performed by Kyoto encyclopedia of genes and genomes (KEGG) pathway analysis and Gene Ontology (GO) term analysis. KEGG analysis revealed that the pathways enriched in miR-155^{high} tumors were mostly immune-related (Supplemental Figure 3A). Consistently, the anti-tumor GO terms, including lymphocyte activation and antigen processing and presentation, were markedly enriched in miR-155^{high} tumors (Supplemental Figure 3B). These results were confirmed by GSEA analysis showing that the immune response signatures, such as lymphocyte activation and interferon (IFN) signaling, were strongly enriched in miR-155^{high} tumors (Figure 3B). Specifically, the expression of T cell functional molecules was dramatically upregulated in the miR-155^{high} tumors (Figure 3C), indicating an augmented anti-tumor immunity within these tumors.

To further confirm the relationship between miR-155 expression and tumor immune profiles, we next applied the CIBERSORTx algorithm (20), which deconvolved the genomic data to estimate the fraction of immune cells in both miR-155^{high} and miR-155^{low} tumor tissues. The correlations between miR-155 expression and total immune cell proportions were generated using the R script. The results showed that miR-155 expression levels in tumors were positively correlated with multiple anti-tumoral immune cell types, including CD8^{+} T cells and M1 macrophages; the results also showed that miR-155 levels were negatively associated with the frequencies of pro-tumoral immune cell types such as regulatory T cells (Tregs) and M2 macrophages (Figure 3D and Supplemental Figure 4). Consistently, using another convolutional neural network-based atlas developed by The

Cancer Image Archive (TCIA) (21), we found that the estimated proportion of tumor infiltrating lymphocytes (TILs) was positively associated with miR-155 level in human breast tumors (Figure 3, E-G).

Together, these data suggest that increased miR-155 levels are positively associated with enhanced innate and adaptive immunity in human breast tumors.

Overexpression of miR-155 in breast cancer cells delays tumor growth and increases anti-tumor immune infiltration

miR-155 in the tumors is derived from both cancer cells and stroma cells including immune cells. While we and others showed the anti-tumor role of immune cell miR-155 (10-19), the role of cancer cell-derived miR-155 is more elusive or controversial (5, 8). To investigate the direct impact of cancer cell-derived miR-155 on tumor progression and tumor immune infiltration, we established B-cell integration cluster (Bic, miR-155 gene) overexpressing breast cancer cell lines (EO771-Bic, 4T1-Bic, and AT-3-Bic) via lentiviral transduction; these cells express 15-60-fold higher miR-155 than control lentiviral transduced cells (EO771-GFP, 4T1-GFP, and AT-3-GFP) (Supplemental Figure 5, A-C). miR-155-overexpressing breast cancer cells exhibited comparable proliferative capacity as the control cells in vitro (Supplemental Figure 5, D-F), as well as similar sensitivities to doxorubicin (Supplemental Figure 5, G and H). Despite these, the growth rate of the tumors with miR-155-overexpressing EO771 cells were significantly delayed compared to EO771-GFP counterparts in C57BL/6 wild type (WT) mice as well as in miR-155 knockout (miR-155^{KO}) mice (Figure 4, A and B). Consistent with our previous report (14), host miR-155 deficiency dramatically accelerated EO771 tumor growth.

We next examined the immune profiles in EO771-Bic and EO771-GFP tumors using flow cytometry. The results showed the frequencies of $CD45^+$ immune cells were significantly increased in EO771-Bic tumors compared to EO771-GFP tumors (Supplemental Figure 6A and Figure 4C). Specifically, overexpression of miR-155 in EO771 breast cancer cells increased the presence of anti-tumor immune cells, including DCs, helper T cells, cytotoxic T cells, and tumoricidal natural killer cells (NK cells) (Figure 4, D and E; Supplemental Figure 6, B-E). Consistently, in 4T1 breast cancer model, overexpressing miR-155 in cancer cells also significantly inhibited tumor growth (Figure 4, F and G), accompanied by increased tumor infiltrating immune cells (Figure 4, H-J), compared to the control counterparts. Additionally, the T cells in EO771-Bic tumors were detected with enhanced proliferative capacity by an in vivo BrdU incorporation assay (Supplemental Figure 6, F and G). Moreover, we discovered an increased number of apoptotic cancer cells in EO771-Bic tumors by both flow cytometry analysis and TUNEL assay, respectively (Supplemental Figure 6, H and I). Concerning immune cell composition, we detected a dramatically lower level of immune infiltration in miR-155^{KO} mice compared to WT mice, which can be explained by their intrinsic defects in CCR5/CXCR3 expression levels (Supplemental Figure 7, A and B).

Our results consistently showed that T cell activation-related genes were drastically upregulated in EO771-Bic tumor infiltrating $CD45^+$ leukocytes isolated from both WT and miR-155^{KO} mice (Supplemental Figure 8 and Figure 4K). Furthermore, IFNγ and TNFα were markedly enriched in the tumor interstitial fluids (TIFs) retrieved from EO771-Bic tumors than from EO771-GFP tumors (Figure 4, L-N).

Taken together, these results, particularly those from the miR-155^{KO} mice, indicate that miR-155 produced by breast cancer cells enhances immune cell influx and anti-tumor capacity, resulting in substantial tumor suppression.

miR-155 overexpression in cancer cells enhances immune cell influx by increasing the production of chemoattractants via suppressing SOCS1 and tilting pSTAT1/pSTAT3 balance

To corroborate the above finding that miR-155 overexpression in breast cancer cells helps flood the tumor with anti-tumor immune cells, we performed an unbiased multiplex proinflammatory chemokine panel assay, to determine the secretome difference between EO771-GFP and EO771-Bic cells. Among 13 types of chemokines tested, we found the concentrations of key chemoattractants for T cell recruitment, including CCL5, CXCL9 and CXCL10 were significantly enriched in EO771-Bic cell conditioned medium (Bic-CM) than that in EO771-GFP cell conditioned medium (GFP-CM) (Supplemental Figure 9, A-C). We next confirmed that miR-155 overexpression upregulated *Ccl5* and *Cxcl9/10/11* expression in murine breast cancer cell lines (Figure 5A; Supplemental Figure 10, A and B) using qPCR. Given that the differential expression of *Cxcl9/10/11* are the highest between GFP and Bic tumor cells, and CXCL9/10/11 share similar regulatory mechanisms and bind to the same receptor CXCR3 (22), we chosen CXCL9 as the representative to investigate how breast cancer cell-derived miR-155 promotes T cell recruitment via upregulating this chemoattractant. We detected that CXCL9 protein levels were remarkably upregulated in miR-155-overexpressing cancer cells in the tumors (Figure 5, B and C) and in cell culture (Supplemental Figure 10, C and D), as well as in the miR-155-overexpressing cell culture

medium (Figure 5D) and EO771-Bic tumor interstitial fluid (TIF) (Figure 5E). Consistent with the murine tumor model, we found in the TCGA database that the expression of T cell recruitment-related genes was substantially increased in miR-155^{high} human breast tumors (Figure 5F) and positively correlated with tumor miR-155 levels (Supplemental Figure 10E).

To confirm if miR-155-overexpressing breast cancer cells attract more activated T cells, we performed an in vitro T cell migration assay using ovalbumin (OVA) peptide (257-264) to stimulate OT-I CD8^{+} T cells, which express high level of CXCR3 (23). As expected, the Bic-CM was more potent in attracting activated T cells than that of GFP-CM, and T cell migration toward GFP-CM and Bic-CM were significantly attenuated and the difference was diminished by CXCR3 blockade (Figure 5, G and H), suggesting the CXCL9/10/11-CXCR3 axis play an essential role in tumor intrinsic miR-155-mediated T cell influx to the tumor.

SOCS1 has been identified as an important miR-155 target (14) and an inhibitor of cytokine-induced signaling that acts via the JAK/STAT pathway (24). Among STAT proteins, STAT1 and STAT3 are reported to regulate the expression of CXCL9/10/11 in myeloid cells (25, 26) and play opposing roles in directing cellular activities (26, 27). To examine whether miR-155 upregulates CXCL9/10/11 expression by targeting SOCS1 and thereby altering downstream STATs, we performed western blot analysis. We found markedly reduced SOCS1 levels accompanied by increased pSTAT1 and STAT1, decreased pSTAT3, and thus increased pSTAT1/pSTAT3 ratio in miR-155-overexpressing EO771, 4T1, and AT-3 tumor cells, compared to control cells (Figure 5, I-K; Supplemental Figure 11, A-C). Importantly, we obtained consistent results using human primary breast cancer cells transduced with lentiviruses to introduce miR-155 overexpression. Specifically, we found

that miR-155 overexpression in human primary breast cancer cells significantly increased *Ccl5* and *Cxcl10/11* expression (Supplemental Figure 12, A-E). In addition, western blot analysis showed a decreased SOCS1, but increased p-STAT1/p-STAT3 levels in miR-155-overexpressing primary cancer cells, compared to controls (Supplemental Figure 12, F-H). To further confirm if SOCS1 is the miR-155 target that regulates CXCL9/10/11 expression via regulating p-STAT1/p-STAT3 balance, we generated SOCS1 knockdown EO771 cells using siRNA transfection (Supplemental Figure 13 A). We found that the EO771 cells with reduced SOCS1 expression displayed similar phenotype with miR-155-overexpressing cells, including enhanced *Cxcl9 and Cxcl11* expression (Supplemental Figure 13, B and C), as well as increased p-STAT1/p-STAT3 ratio (Supplemental Figure 13, D-F).

These data indicate that the increased pSATA1/pSTAT3 ratio may have led to increased CXCL9/10/11 expression in miR-155-overexpressing breast cancer cells. Indeed, STAT3 inhibition by Stattic phenocopied miR-155 overexpression and enhanced CXCL9 production in breast cancer cells (Figure 5, L and M; Supplemental Figure 11D).

Taken together, these results suggest that miR-155 in breast cancer cells enhances CXCL9/10/11 expression by suppressing SOCS1 expression and tilting the pSTAT1/pSTAT3 ratio, leading to the recruitment of effective T cells to the tumor site and subsequently an improved anti-tumor immune response.

miR155 deficiency promotes tumor progression by impairing immune cell recruitment

To further verify above findings, we generated miR-155 knockout (miR-155^{KO}) EO771 cells using the CRISPR-Cas9 genomic editing system. miR-155 level in miR-155^{KO} cells was decreased by about 75 % (Figure 6A), without affecting cell proliferation in vitro (Figure 6, B

and C). We speculate that miR-155 was not completely eliminated in the cells due to the endocytosis of miR-155 in FBS contained in the culture medium, as the sequence of miR-155 is highly conserved among many species (28). We obtained opposite results to what we found in EO771-Bic cells, including significantly reduced *Ccl5* and *Cxcl9/10/11*expression in miR-155^{KO} EO771 cells (Figure 6D). In addition, we also detected decreased level of intracellular CXCL9 at the protein level via flow cytometry (Figure 6, E and F). Importantly, miR-155^{KO} EO771 tumors grew faster in vivo, compared with their control counterparts (Figure 6, G and H). Immune profile analysis displayed reduced immune cells (Figure 6I), including anti-tumor CD8^{+} T cell (Figure 6, J-L) accumulation in tumor tissues. Mechanistically, we detected an increase in SOCS1 but a decrease in the p-STAT1/p-STAT3 ratio in miR-155^{KO} EO771 cells (Figure 6, M-O).

Taken together, our in vitro and in vivo data using miR-155^{KO} tumor cells further confirmed the anti-tumor role of endogenous miR-155 in regulating anti-tumor immune response by targeting SOCS1 and altering its downstream p-STAT1/p-STAT3 balance.

miR-155^{high} tumors have elevated expression of immuno-break molecules

Emerging evidence has revealed that increased expression of immunosuppressive molecules is concomitant with an activated immune response. This negative feedback loop is essential for maintaining normal immune responses and limiting T cell activity to protect normal cells during chronic inflammation (29, 30). However, tumors may circumvent T cell-mediated cytotoxicity by expressing immunosuppressive molecules on both cancer cells and tumor-infiltrating immune cells, resulting in the inhibition of immune-mediated cancer cell death (30).

GSEA analysis of TCGA database showed that the negative regulators of immune response and lymphocyte apoptotic processes were highly enriched in miR-155^{high} human breast tumors (Figure 7A). Specifically, the expression of hallmark immunosuppressive genes including *PDCD1* (PD1), *CD274* (PD-L1), *CTLA4*, and *FOXP3* was drastically upregulated in miR-155^{high} tumors (Figure 7B). Consistent with the TCGA data, we found that in CD45^{+} leukocytes isolated from EO771-Bic tumors in both WT and miR-155^{KO} mice, the overall expression of main checkpoint molecules was substantially increased (Figure 7C). Furthermore, the concentrations of soluble PD-L1 in the TIFs harvested from Bic tumors were significantly higher than those from control GFP tumors (Figure 7D). In addition, not only the expression of PD-L1 on miR-155-overexpressing human primary and murine breast cancer cells was upregulated (Supplemental Figure 14, A-F), but also the expression of PD-L1 on tumor associated macrophages (TAMs) was significantly upregulated in Bic tumors compared to that in control GFP tumors (Supplemental Figure 14, G-J).

These data suggest that the enhanced antitumor immunity elicited by cancer cell miR-155 overexpression also triggers immunosuppressive pathways in breast tumors, which may set a stage for ICB therapy.

Tumors with miR-155-overexpressing cancer cells display an improved response to immunotherapy and elicit a stronger immunological memory

The elevated expression of immuno-break molecules in miR-155^{high} tumors prompted us to explore if elevated miR-155 levels in breast cancer cells could sensitize the tumors to ICB therapy. We treated established EO771-GFP and EO771-Bic tumors with anti-PD-L1 monoclonal antibodies (αPD-L1 mAbs) and observed that EO771-Bic tumors were more

sensitive throughout the treatment cycle, as determined by percentage of tumor inhibition (Figure 7, E and F).

Abundant evidence indicates that exosomes carrying bioactive miRNAs that can shuttle between tumor cells and other types of cells in the TME, therefore affecting many aspects of tumor development, including immune cell activities (31, 32). Based on recent findings indicating that miR-155 is anti-tumoral in multiple immune cells (2, 8, 10-15, 18, 19), we hypothesized that the exosomes containing miR-155 produced by tumor cells may directly facilitate immune cell activation in the TME. To address this question, we purified exosomes from EO771-GFP and EO771-Bic tumor-conditioned media by differential centrifugation (Supplemental Figure 15A). miR-155 level in Bic cell-derived exosomes (Bic-Exo) was about 150-fold higher than that in GFP cell-derived exosomes (GFP-Exo) (Supplemental Figure 15B). To investigate if tumor-derived exosomal miR-155 affects anti-tumor immunity in vivo, we injected a single dose of 50 μg of each exosome type intravenously (i.v.) into EO771 tumor-bearing mice (Supplemental Figure 15C). Three days later, we analyzed the immune profile within tumors and tumor-draining lymph nodes and found that Bic-Exo administration elicited an enhanced anti-tumor immune response, characterized by augmented immune response in tumor draining lymph nodes (Supplemental Figure 15, D-F), as well as increased presence of overall $CD45^+$ immune cells (Supplemental Figure 15G) and cytotoxic $CD8^+$ T cells in tumor tissues (Supplemental Figure 15, H-J).

To explore if miR-155 overexpression in cancer cells elicits immune memory in tumor-bearing mice, we surgically removed EO771-GFP or EO771-Bic tumors 20 days post-inoculation and re-challenged the same mice with parental EO771 cells in the contralateral

mammary fat pad and with B16-F10 melanoma cells on the back, and then monitored the growth of the new EO771 and B16-F10 tumors. (Supplemental Figure 16A). Some naïve mice were also challenged with parental EO771 and B16-F10 tumors as control. The results showed that the mice which previously had EO771-GFP tumors displayed a modest increase in tumor-specific immune memory, which curbed the growth of the reinoculated breast tumors compared to those in the control naive mice, but without statistical significance (P = 0.12 on day 17); however, melanoma progression in these mice was observed to be accelerated. Interestingly, the mice that previously had EO771-Bic tumors almost completely rejected both newly transplanted EO771 tumors and B16-F10 melanomas (Supplemental Figure 16, B and C), and their survival time was dramatically extended (Supplemental Figure 16D). These data suggest that to a certain extent, EO771-GFP tumors established immunological memory to the same cancer type, but the immunosuppressive metabolites released by invasive tumors might also compromise systemic immune function, which would then favor the development of a different type of tumor.

Serum miR-155 level mirrors the immune status of breast tumors

Tumor-derived nucleic acids, including miRNAs, have recently been proposed as diagnostic and prognostic biomarkers (33, 34). miR-155 was not only highly enriched in tumor-derived exosomes as above mentioned (Supplemental Figure 15B) but also detectable in the non-concentrated cell culture media (Supplemental Figure 17, A-C). To test the feasibility of using circulating miR-155 level as a prognostic biomarker, we then measured the miR-155 levels in serum of tumor-bearing mice. miR-155 was measured in the serum with significantly higher levels in EO771-Bic tumor-bearing mice than in EO771-

GFP tumor-bearing mice (Figure 8A). Notably, the levels of serum miR-155 of WT and KO mice were comparable in mice with either EO771-GFP tumors or EO771-GFP tumors (Figure 8A). This suggests that breast cancer cells were the main source of serum miR-155 in these mice. A significant association was observed between serum miR-155 levels and the frequency of tumor infiltrating $CD8^+$ T cells in the tumors of miR-155^{KO} mice (Figure 8B). In addition, serum miR-155 levels were positively correlated with the protein levels of chemoattractant CCL5 and CXCL9 (Figure 8, C and D), immune activating IL-12 (Figure 8E), and immunosuppressive PD-L1 (Figure 8F) in the TIFs of the miR-155^{KO} mice.

To explore the potential value of circulating miR-155 levels in evaluating the immune status of human breast tumors, we harvested matched sera and tumor tissues from a small cohort of patients with breast cancer (Figure 8G and Supplemental Table 1). Using qPCR to analyze miR-155 expression levels, we observed that while serum miR-155 levels did not correlate with normal breast tissue miR-155 expression levels (Supplemental Figure 18), they faithfully reflected the miR-155 expression levels in breast tumor tissue (Figure 8H). Moreover, serum miR-155 levels were also positively correlated with the expression levels of hallmark anti-tumor immune activation genes *IL2*, *CD8A*, and *IFNG* (Figure 8, I-K). Notably, serum miR-155 abundance also mirrored the expression levels of the immunosuppressive molecule, *CD274* (*PD-L1*), in tumor tissues (Figure 8L).

Taken together, these results indicate that circulating miR-155 can serve as a non-invasive biomarker in estimating the immune status of breast tumors, and therefore may be of great value in predicting their prognosis and response to ICB treatment.

Discussion

miR-155 is a multifunctional molecule and plays intricate, and sometimes contradictory, roles in various cancers (7-9, 35-37). Recent findings of our group and others have revealed the pivotal role of immune cell expressed miR-155 in anti-tumor immunity (10-15, 18, 19), while the functions of miR-155 expressed in breast cancer cells are more elusive. As the dynamic crosstalk between malignant and immune cells in the TME has a profound impact on tumor progression (38), in this study we particularly sought to examine how breast cancer cell-derived miR-155 affects immune cell phenotype and functionality.

By analyzing human breast cancer data from multiple repositories in respect to miR-155 expression, we first demonstrated a correlation between higher miR-155 levels and favorable anti-tumor immune infiltrations in human breast tumors, as well as better patient prognosis. To dissect a potential causative relationship, we investigated the direct role of cancer cell miR-155 in enhancing anti-tumor immunity using murine breast cancer models. It was found that overexpression of miR-155 in breast cancer cells significantly delayed tumor progression via increasing the recruitment of effector immune cells to the TME. Since this happened also in miR-155 deficient mice which lack of host miR-155 expression, the tumor-suppressive function of miR-155 overexpression in breast cancer cells is likely independent of miR-155 expression in immune cells. Furthermore, we found that miR-155 is secreted from breast cancer cells to the TME and circulation and thus circulating miR-155 may be utilized as a biomarker for evaluating the immune status of breast cancer patients.

There are some conflicting reports regarding the role of miR-155 in breast cancer development and progression. miR-155 expression levels in breast cancer have been

shown to be associated with high-grade, advanced stage, metastases, and invasion (35, 39). However, a study on a large series of triple-negative breast cancers showed that high miR-155 levels decreased the efficiency of homologous recombination repair by targeting the recombinase RAD51, thus were associated with better overall survival of patients (7). Another study reported that stable expression of miR-155 in 4T1 murine breast cancer cells significantly reduced the aggressiveness of tumor cell dissemination by preventing tumor cell epithelial-to-mesenchymal transition (EMT) in vivo (40). The seemingly contradicting conclusions reached in previous miR-155 studies may be attributed to variations in sample size, cancer types, animal models, and experimental design. Notably, we showed that even when miR-155 was expressed in breast cancer cells at a level 60-fold higher than baseline, it did not affect breast cancer cell proliferation and sensitivity to chemotherapy drug doxorubicin.

We investigated the mechanism by which cancer cell miR-155 overexpression enhances anti-tumor immunity in breast tumors. Chemotactic cytokines and chemokines determine the migratory behavior of immune cells. Regarding the tumors, it has been well studied that CXCL9/10/11 (ligands for CXCR3) produced by macrophages and DCs, along with CCL5 (ligands for CCR5) secreted by tumor cells are associated with T cell recruitment to the TME and a favorable response to chemotherapy and immunotherapy (41, 42). We observed that miR-155 dramatically upregulated CCL5 and CXCL9/10/11 expression in breast cancer cells. Accordingly, we also noted that conditioned medium from miR-155-overexpressing cells recruited more OVA activated OT-1 T cells in vitro, suggesting that

tumor cells with high miR-155 expression recruit more effective T cells to tumor site and turn "cold" tumors "hot", which may provide better targets for immunotherapy.

These findings prompted us to explore the intrinsic cellular signaling events regulated by miR-155. STATs are responsible for chemokine and cytokine production, which can be regulated by SOCS1. As SOCS1 is a direct miR-155 target, we hypothesized that miR-155 might increase CXCL9/10/11 expression by suppressing SOCS1 and thus regulating STATs activities. Indeed, we detected increased STAT1 expression and activation, but decreased phosphorated STAT3 levels in miR-155 overexpressing cancer cells. Depending on the context, STAT1 and STAT3 play opposing roles and regulate one another via SOCS1. We confirmed the above regulatory mechanisms using human primary breast cancer cells overexpressing miR-155, miR-155^{KO} EO771 cells, as well as SOCS1 depleted EO771 cells. In addition, we also observed in our in vitro study that a STAT3 inhibitor increased CXCL9 expression in tumor cells, indicating the balance of pSTAT1/pSTAT3 was a determinant in regulating chemokine production in tumor cells.

Upon tumor-specific T cell activation, released interferons trigger the inducible expression of immunosuppressive molecules by cancer cells or myeloid cells in the TME, thereby leading to T cell exhaustion and restricting the antitumor immune response, which is known as adaptive immune resistance (43). In the mice bearing miR-155-overexpressing tumors, along with the enhanced anti-tumor immune cell infiltration, a concomitant increase of immune-suppressive molecules, including PD-L1 and CTLA4, occurred. This would be expected to limit antitumor activity. These immune checkpoint genes were also found to be upregulated in miR-155^{high} tumors from human breast cancer patients. We also discovered

that miR-155 overexpression intrinsically increased PD-L1 expression in both human primary breast cancer cells and murine breast cancer cell lines, which may explain our in vivo findings showing the miR-155-overexpressing tumors are sensitive to ICB therapy. The establishment of immunological memory is an important aspect of durable antitumor responses against tumor relapse (29). In our study, we demonstrated that tumor-derived miR-155 was highly enriched in exosomes, which can significantly strength the anti-tumor immune response when applied to tumor bearing mice intravenously. We speculate that tumor-derived exosomal miR-155 may help the host to establish an augmented immune protective mechanism as we observed that tumors with miR-155 overexpression elicited a stronger systemic immunological memory, resulting in rejection of rechallenged tumors after surgical removal of primary tumors.

Exist in free form or embedded in macrovesicles, like above mentioned exosomes, miRNAs can be secreted into the circulation and exist in remarkably stable forms (34). An abundance of circulating miRNAs is in some cases associated with the initiation and progression of cancer and can be easily detected via basic molecular biology techniques (34, 44). Therefore, considerable effort has been devoted to identifying suitable circulating miRNAs as noninvasive biomarkers not only for early cancer diagnosis, but also as a predictor of prognosis and treatment response (33, 34). Our data showed that breast cancer cell-derived miR-155 can be released into peripheral blood, and that serum miR-155 levels not only mirror the tumor miR-155 expression, but also reflect the anti-tumor status in the TME. These data suggest the potential of utilization of circulating miR-155 levels in patients

with breast cancer as a prognostic biomarker, as well as a predictive marker for the efficacy of ICB therapies.

Also importantly, because this study showed that the forced overexpression of miR-155 in breast cancer cells led to improved anti-tumor immunity accompanied by elevated expression levels of immune checkpoint molecules in breast tumors, we envision that nanotechnology or virus-based therapeutic strategies to increase miR-155 expression in breast tumors may enhance the efficacy of ICB therapies. A limitation of this study is that we based our conclusions on syngeneic breast cancer mouse models. In future studies, we will use humanized mice engrafted with human breast tumors to confirm our findings.

In conclusion, our study suggests that breast cancer cell expressed miR-155 plays an anti-tumor role by enhancing anti-tumor immune responses, serum miR-155 levels can be used as a predictive biomarker for patient prognosis and their response to immune therapy and boosting miR-155 expression in breast tumors could be a promising therapeutic strategy, particularly when it is used in combination with ICBs.

Methods

Bioinformatic analysis

RNA-Seq, miRNA-Seq data and clinical information of human breast cancer were retrieved from the GDC portal (https://portal.gdc.cancer.gov/). After normalization using "limma" R package, the expression data of miRNA-Seq and RNA-Seq were aligned to the clinical information of breast cancer patients (n = 995). miR-155^{high} and miR-155^{low} groups were separated based on the median value of miR-155 expression in tumors, unless otherwise noted. The differentially expressed genes (DEGs) between these two groups were extracted using "DESeq" R package and the result was visualized in a volcano plot. The parameters set for differential expression analysis were FDR < 0.05 with |Log2FC| > 1. Cox regression analysis was performed to assess the prognostic association of hsa-miR-155 expression, adjusted for age, sex, race, tumor stage, and tumor purity. The tumor purity was estimated by ESTIMATE (45) and the association analysis were performed on the platform of SCISSOR™ (46). Hazard ratio, 95% confidence interval (CI), and p-value were calculated. The association of hsa-miR-155 expression with survival in each of five main intrinsic subtypes (Luminal A, Luminal B, HER2, Basal-like and Normal-like), which were defined by PAM50 (47) was investigated. The patient survival data of EGA (European Genome-Phenome Archive) repository (48) and GEO (Gene Expression Omnibus) datasets (49) were obtained from Kaplan-Meier Plotter (KM plotter) (50). For survival analysis, Kaplan-Meier plot was generated by using "survival" and "survminer" R packages and examined by using log-rank test.

Pathway enrichment analysis

A total of 12,888 genes with normalized values were analyzed for pathway and gene signature enrichment analysis. Gene ontology (GO) and Kyoto Encyclopedia of Genes and Genomes (KEGG) pathway enrichment analysis were performed and visualized via “GOplot” and “ggplot2” R packages. Gene set enrichment analysis (GSEA) was performed using the GSEA software (version 4.0.3) with the default settings and 1,000 gene set permutations. Gene sets used in these analyses were derived from the Molecular Signature Database (MSigDB) (51). Multi-GSEA plots were generated using “ggplot2” R package.

Immune cell infiltration with CIBERSORTx

CIBERSORTx was applied to estimate the immune cell composition of breast cancer tumor tissues based on a validated leukocyte gene signature matrix and default settings. The normalized gene expression profile of the TCGA data was input into CIBERSORTx for analysis based on a deconvolution algorithm with 100 permutations and S-batch correction to remove variances between different sequence platforms. To control the accuracy of the deconvolution algorithm, data with a $P < 0.05$ was screened for the following analysis.

Patients and specimens

All clinical sample collections were conducted according to the Declaration of Helsinki principles. Matched tumor samples for serum and tumor miR-155 expression analysis were obtained from patients with pathologically confirmed breast cancer at Nanjing Drum Tower Hospital, the Affiliated Hospital of Nanjing University Medical School. None of the patients received anticancer therapy prior to sampling. Paired serum, non-tumor (taken at least 3 cm

distal to the tumor site), and tumor tissues from 29 breast cancer patients who underwent a tumor resection (Supplementary Table 1) were used to extract RNA. The TNM staging was classified according to the 8th edition of the American Joint Committee on Cancer (AJCC). Triple negative breast cancer samples for primary cancer culture were obtained from Cancer Institute of Prisma Health (Greenville, SC).

Mice

All mice used for this study were 6-8 weeks old females, including C57BL/6 wild type (WT), miR-155 KO, and OT-1 mice, all of which were obtained from Jackson Laboratories (Bar Harbor, Maine). Mice were maintained in pathogen-free conditions at the University of South Carolina according to National Institutes of Health guidelines.

Cell culture and tumor conditioned medium collection

Breast cancer cell lines EO771 (American Type Culture Collection (ATCC), CRL-3461), 4T1 (ATCC, CRL-2539) and AT-3 (Sigma-Aldrich, SCC178), and melanoma cell line B16-F10 (ATCC, CRL-6475) were expanded in high-glucose Dulbecco's modified eagle medium (DMEM, Sigma-Aldrich, D6429) supplemented with 10% fetal bovine serum (FBS, Gibco, A4766801), 100 U/mL penicillin, and 100 µg/mL streptomycin (Gibco, 15140148). All cells were maintained in a humidified, 5% CO_2 incubator at 37˚C.

For in vitro CXCL9 level determination, tumor cells were treated with Stattic (Sigma-Aldrich, S7947) as indicated, and then cells were trypsinized and harvested for flow cytometry. For chemo-sensitivity assay, tumor cells were treated with doxorubicin for 24 hours, cell viability was determined by MTT assay (Sigma-Aldrich, CT02) according to the manufacturer's instructions.

Tumor-conditioned medium was prepared by plating 6 × 10^6 tumor cells in 10 cm dishes. The medium was changed to serum-free DMEM for another 48 hours when cells were 80% confluent. The supernatant harvested was filtered by 0.45 μm strainer and stocked in -80 ˚C as tumor-conditioned medium.

miR-155 overexpressing tumor cell lines establishment

Details of lentiviral vector construction and lentiviral transduction have been reported previously (14, 15). Forty-eight hours after transduction, GFP^+ cells were sorted for the subsequent experiments.

miR-155 knockout cell generation by CRISPR-Cas9

For the generation of lentiviral-based miR-155knock out via CRISPR/Cas9, EO771 cells were transfected with empty lentiCRIPSR or lentiCRISPR containing dual-gRNA (5'-GTTGCATATCCCTTATCCTC-3' and 5'-GACATCTACGTTCATCCAGC-3') targeting miR-155. After limiting dilution, single clone was selected out in the presence of puromycin (2 μg/mL) for three weeks. qPCR was performed to validate the successful miR-155 knockout in EO771 cells before using for downstream experiments.

Human primary breast cancer cell isolation and culture

Triple negative human breast cancer cells were isolated and cultured as previously reported (52). Briefly, tumor tissue was mechanically cut into small pieces (< 1 mm^3) using scalpels and enzymatically dissociated in a mixture of collagenase/hyaluronidase (STEMCELL Technologies, 07912) for 16 hours at 37 ℃, following by further digestion with trypsin (0.25%) for 2 min and then 5 units/ml of dispase (STEMCELL Technologies, 07913) and 0.05 mg/ml of DNase I (STEMCELL Technologies, 07900) for 1 min. After centrifugation

at 150 × g for 5 min, cells were seeded at density 1 × 10^5/well onto Geltrex™ (23 μg of protein per 1 cm^2; Thermo Fisher Scientific, A1413202) coated six-well plates in human complete EpiCul™-B medium (STEMCELL Technologies, 05602, 05630 and 07925). Cells were either further cultured or passaged using trypsin–EDTA (0.25%) for downstream usage.

Tumor models

Mouse orthotopic breast cancer models were established as previously described with a minor modification (12, 14). Briefly, 2 × 10^5 EO771 cells suspended in 10 μl PBS were implanted into the 4th pair of mammary fat pads of mice. To establish subcutaneous melanoma in mice, 1 × 10^6 B16-F10 cells in 10 μl of PBS were implanted into the rear flanks of mice. The tumor size was monitored by caliper on indicated days. Tumor volume was calculated according to the following formula: Tumor volume ≈ $(\text{short axis})^2 \times (\text{long axis})/2$. To determine tumor sensitivity to immunotherapy, anti-mouse PD-L1 mAb (100 μg/mouse, BioXcell, BP0101) was applied to mice with established EO771-GFP or EO771-Bic tumors intravenously on day 12, day 15, and day 18 post tumor inoculation; IgG2b was used as isotype control (BioXcell, BP0090). Tumor volume was monitored. Tumor sensitivity to anti-PD-L1 treatment was determined using the following formula: % of tumor inhibition = $\frac{\text{Tumor volume (IgG2b)} - \text{Tumor volume (anti-PD-L1)}}{\text{Tumor volume (IgG2b)}} \times 100$. At the experimental end point, mice were sacrificed. Tumors and tumor-draining lymph nodes were removed, weighed, and processed for subsequent experiment.

Cell isolation and interstitial fluid collection

Cells from mouse spleens were isolated by mechanical disruption. Tissue-infiltrating leukocytes were obtained as described previously (14, 53). In short, fresh resected tumor

specimens were minced and enzymatically digested in completed RPMI 1640 medium (Sigma-Aldrich, R8758) supplemented with 0.3 mg/ml of collagenase, Type 4 (Worthington, LS004189), 200 U/ml of DNase I (Worthington, LS006334), and 1U/ml of Hyaluronidase (Sigma-Aldrich, H3506) for 1 h at 37°C. Cells were thoroughly rinsed with ice-cold PBS, then erythrocytes were lysed using red blood cell lysing buffer (Sigma-Aldrich, R7757), per manufacturer's instructions. Dissociated cells were passed through a 70-μm cell strainer and resuspended in medium supplemented with 1% FBS for flow cytometry analysis.

Tumor infiltrating leukocytes were isolated using EasySep™ Mouse PE Positive Selection Kit (STEMCELL Technologies,17696) following manufacturer's instruction. Splenic T cells were isolated using EasySep™ Mouse T cell isolation Kit (STEMCELL Technologies,19851) following manufacturer's instructions. In all sorted samples, a purity of > 95% was achieved as determined by flow cytometry.

To collect tissue interstitial fluid, tumors were freshly harvested and cut into small pieces. Samples were then vortexed in serum free DMEM (0.5 g tissue/ml medium) for 30 seconds to dissolve the interstitial fluid and centrifuged at 450 × g for 5 min. The resulting supernatant was collected and filtered through a 0.22-μm filter to remove any debris. The obtained liquid was referred to as tissue interstitial fluids (TIFs).

Flow Cytometry

Flow cytometry was performed as previously described (14, 53). For surface staining, the in vitro cultured and tissue-infiltrating cells were stained with fluorochrome-conjugated antibodies (Abs) for 30 min, then washed and analyzed via flow cytometry. For intracellular staining, cells were stimulated with or without Cell Activation Cocktail (Biolegend, 423304),

depending on the experiment's needs, followed by BD fixation and permeabilization treatment via manufacturer protocols. Samples were then incubated with fluorochrome-conjugated Abs for 30 min, washed, and resuspended in wash buffer. To measure cell proliferation capacity, we performed a BrdU incorporation assay. For in vitro labeling, 1 μM of BrdU was applied 30 min prior to harvesting. For in vivo labeling of mouse cells, 1 mg BrdU in 200 μl of PBS was injected intraperitoneally 24 hours prior harvesting. All samples were then processed according to the manufacturer's directions (BD Biosciences, 559619). To evaluate apoptosis, cells were incubated with 5 μg/ml of propidium iodide (PI, Biolegend, 421301) for 15 minutes before analysis. Data was acquired and read on a BD FACS Aria II flow cytometer and analyzed using Flowjo software 10.8.0 (BD Biosciences). Details of the fluorochrome conjugated Abs that were used in this study are listed in Supplementary Table 4.

Quantitative real-time PCR (qPCR) for mRNA and miR-155 expression

Tissues/cells were lysed in 700 μl Qiazol lysis reagent (QIAzol), and tissue samples were homogenized. RNA was extracted using Qiagen miRNeasy Mini Kits (217084) to allow for the collection of microRNAs and mRNAs. cDNA was then synthesized with 1 μg RNA using miScript II RT kits (Qiagen, 218161). miR-155 expression was measured by a Bio-Rad CFX96 thermocycler using miScript SYBR Green PCR kits (Qiagen, 1046470) according to the manufacturer's instructions. Qiagen miScript Primers were purchased for Mmu-miR-155 (mouse, MS00001701), Hsa-miR-155 (human, MS00003605), and RNU6 (MS00033740). For normalization, miR-155 expression was presented relative to RNU6 expression.

For mRNA expression detection, qPCR was performed using iQ™ SYBR® Green Supermix (Bio-Rad, 1708880). All primers used for qPCR analysis of genes were synthesized by Integrated DNA Technologies (Coralville, IA). The primer sequences are listed in Supplemental Table 5. The relative amount of target mRNA was determined using the comparative threshold (Ct) method by normalizing target mRNA Ct values to those of 18s rRNA.

LEGENDplex™ assay

To investigate the cytokine/chemokine profile in the secretomes of the EO771-GFP and EO771-Bic cells, we performed a multiplex proinflammatory chemokine panel assay (Biolegend, 740451) according to the manufacturer's instructions. The concentration of chemokines was quantified using The LEGENDplex™ Data Analysis Software Suite.

ELISA (enzyme-linked immunosorbent assay)

The concentrations of IFNγ (Biolegend, 430804), TNFα (Biolegend, 430904), CCL5 (R&D, DY478-05), CXCL9 (R&D, DY492-05), and soluble PD-L1 (R&D, DY1019-05) in tumor-conditioned media or tumor interstitial fluids were determined using ELISA kits according to the manufacturers' instructions.

In vitro T cell activation and migration

T cell activation and migration assays were performed following the protocol by Albert et al.(23). Briefly, splenocytes from OT-1 transgenic mice were stimulated with 1 nM TCR-specific peptide Ovalbumin (257-264) (Sigma-Aldrich, S7951) for 1 h. Seven days post culture in complete RPMI 1640 medium with 50 U/ml of recombinant IL-2 (R&D, 402-ML-020/CF), $CD8^+$ T cells with high CXCR3 expression were used for T cell migration assay.

To inhibit receptor binding of CXCR3, anti-mouse CXCR3 mAb (10 µg/ml, BioXcell, BE0249) was applied to treat activated OT-1 cells for 1 h at 37˚C; IgG2b (10 µg/ml, BioXcell, BP0090) pretreated cells were used as isotype control. Then, 0.1×10^6 activated T cells were placed into 5 µm pore size polystyrene trans-well inserts (Corning, 3421) in serum-free RPMI-1640 and allowed to migrate for 1.5 h at 37˚C towards EO771-GFP/Bic cell conditioned medium. Cells that had migrated to the receipt chamber were collected and counted using Precision Counting Beads™ (Biolegend, 424902) by flow cytometry.

TUNEL assay

Apoptosis in tumor sections was determined using In Situ Cell Death Detection Kit, according to the manufacturer's instructions (Roche, C755B40). Dead cells were quantified by counting the number of $TUNEL^+$ cells in 10 fields for each section.

Western blotting

In vitro cultured cancer cells from independent dishes were dissolved in RIPA cell lysis buffer (ThermoFisher, 89901) supplemented with a protease inhibitor (Sigma-Aldrich, P8340) and a phosphatase inhibitor (Sigma-Aldrich, P00441). The protein concentrations were determined using a Rapid Gold BCA protein assay kit (ThermoFisher, A53227). In each group, Equal amounts of protein were separated by SDS/PAGE and transferred to a 0.22 or 0.45 µM nitrocellulose (50) membrane by electroblotting. Samples were loaded either on the same gel or separate gels. For antigens that detected on different blots, separated loading controls were applied. The indicated Abs (Supplementary Table 6) were applied, and the protein bands were determined using ECL Plus reagent (ThermoFisher, 32132). Western

blotting bands were quantified using ImageJ software relative to internal control (β-Actin) expression.

SOCS1 knockdown by siRNA

To silent SOCS1 expression, EO771 cells were transfected with 10 nM of siRNA target mouse SOCS1 (OriGene, SR426031) using Lipofectamine® RNAiMAX Reagent (Invitrogen, 13778) according to the manufacturer's instructions. 48 hours post transfection, cells were harvested for downstream analysis.

Exosome purification and in vivo administration

For exosome purification from EO771-GFP/Bic cell conditioned media, extracellular vesicles were purified by a standard differential centrifugation protocol. In brief, culture supernatants were centrifuged at 2,000 × g for 10 min to remove cell debris and dead cells. Microvesicles were next pelleted by centrifugation at 10,000 × g for 30 min. Supernatants were then centrifuged at 160,000 × g for 90 min at 4 °C. The pelleted exosomes were suspended in PBS. The size distribution of isolated exosomes was measured using nanoparticle tracking analysis. The purified exosomes were quantified by determining protein concentrations using a Rapid Gold BCA protein assay kit (ThermoFisher, A53227).

For in vivo study, GFP or Bic exosomes with 50 μg of protein equivalent in 100 μl of PBS were injected via retro-orbital venous plexus on EO771 tumor bearing mice. Three days later, tumors and tumor-draining lymph nodes were removed for immune profile analysis.

Statistics

Data was shown as mean ± standard error of mean (SEM) whenever the mean was the primary value representative of a sample group's behavior. Two group comparison was

accomplished using a two-tailed Student's *t* test or Wilcoxon rank sum test as indicated. One-way ANOVA followed by Tukey's post-hoc test was used for multiple comparisons. Two-way ANOVA with Tukey's post-hoc test was used to analyze the tumor growth data. The cumulative survival time was estimated using the Kaplan-Meier method. The survival association analysis was performed using the Cox proportional hazards model. The comparisons were performed using GraphPad Prism 9 (Graphpad Software Inc.) or R. $P \leq 0.05$ was considered statistically significant for all tests.

Study approval

All animal experiments were approved by the Institutional Animal Care and Use Committee (IACUC) at the University of South Carolina. For experiments using human breast cancer specimen, all samples were anonymously coded as stipulated by the Declaration of Helsinki. Written informed consent was obtained from the patients prior to inclusion in the study. The use of human subjects for this study was approved by the Institutional Review Board (IRB) of Nanjing Drum Tower Hospital and Prisma Health.

Author contributions

JW and DF designed the experiments. JW, QW, XW, KL and YW performed experiments, analyzed, and interpreted the data. GY, YS and YY provided clinical samples and collected data of human specimen. JW and GC performed bioinformatics analysis. ML, JK, EAM and YY helped in data interpretation. JW, KL and DF wrote the manuscript, and all authors contributed to editing of the manuscript.

Acknowledgments

The authors wish to thank Ms. Kia Zelars for help with cell sorting. The graphic abstract and all schematic figures in this study were partially created with BioRender.com. This work was supported by the National Institute of Health grants R01CA218578 (to DF and EAM) and R21CA216230 (to DF).

References

1. Wu M, et al. MiR-155-5p promotes oral cancer progression by targeting chromatin remodeling gene ARID2. *Biomed Pharmacother*. 2020;122:109696.

2. Pedersen IM, et al. Onco-miR-155 targets SHIP1 to promote TNFalpha-dependent growth of B cell lymphomas. *EMBO Mol Med*. 2009;1(5):288-95.

3. Gironella M, et al. Tumor protein 53-induced nuclear protein 1 expression is repressed by miR-155, and its restoration inhibits pancreatic tumor development. *Proc Natl Acad Sci U S A.* 2007;104(41):16170-5.

4. Babar IA, et al. Inhibition of hypoxia-induced miR-155 radiosensitizes hypoxic lung cancer cells. *Cancer Biol Ther.* 2011;12(10):908-14.

5. Zhang Y, et al. Hepatitis C virus-induced up-regulation of microRNA-155 promotes hepatocarcinogenesis by activating Wnt signaling. *Hepatology*. 2012;56(5):1631-40.

6. Cai ZK, et al. microRNA-155 promotes the proliferation of prostate cancer cells by targeting annexin 7. *Mol Med Rep.* 2015;11(1):533-8.

7. Gasparini P, et al. Protective role of miR-155 in breast cancer through RAD51 targeting impairs homologous recombination after irradiation. *Proc Natl Acad Sci U S A.* 2014;111(12):4536-41.

8. Ekiz HA, et al. MicroRNA-155 coordinates the immunological landscape within murine melanoma and correlates with immunity in human cancers. *JCI Insight.* 2019;4(6): e126543.

9. Pu J, et al. Adrenaline promotes cell proliferation and increases chemoresistance in colon cancer HT29 cells through induction of miR-155. *Biochem Biophys Res Commun*. 2012;428(2):210-5.

10. Zonari E, et al. A role for miR-155 in enabling tumor-infiltrating innate immune cells to mount effective antitumor responses in mice. *Blood*. 2013;122(2):243-52.

11. Monnot GC, et al. miR-155 Overexpression in OT-1 CD8(+) T Cells Improves Anti-Tumor Activity against Low-Affinity Tumor Antigen. *Mol Ther Oncolytics.* 2020;16:111-123.

12. Wang J, et al. MicroRNA-155 deficiency enhances the recruitment and functions of myeloid-derived suppressor cells in tumor microenvironment and promotes solid tumor growth. *Int J Cancer.* 2015;136(6):E602-13.

13. Yu F, et al. miR-155-deficient bone marrow promotes tumor metastasis. *Mol Cancer Res.* 2013;11(8):923-36.

14. Wang J, et al. microRNA-155 deficiency impairs dendritic cell function in breast cancer. *Oncoimmunology.* 2016;5(11):e1232223.

15. Hodge J, et al. Overexpression of microRNA-155 enhances the efficacy of dendritic cell vaccine against breast cancer. *Oncoimmunology*. 2020;9(1):1724761.

16. He M, et al. MicroRNA-155 regulates inflammatory cytokine production in tumor-associated macrophages via targeting C/EBPbeta. *Cell Mol Immunol.* 2009;6(5):343-52.

17. Vigorito E, et al. microRNA-155 regulates the generation of immunoglobulin class-switched plasma cells. *Immunity.* 2007;27(6):847-59.

18. O'Connell RM, et al. MicroRNA-155 promotes autoimmune inflammation by enhancing inflammatory T cell development. *Immunity.* 2010;33(4):607-19.

19. Dudda JC, et al. MicroRNA-155 is required for effector CD8+ T cell responses to virus infection and cancer. *Immunity.* 2013;38(4):742-53.

20. Newman AM, et al. Determining cell type abundance and expression from bulk tissues with digital cytometry. *Nat Biotechnol.* 2019;37(7):773-782.

21. Clark K, et al. The Cancer Imaging Archive (TCIA): maintaining and operating a public information repository. *J Digit Imaging*. 2013;26(6):1045-57.

22. Humblin E, Kamphorst AO. CXCR3-CXCL9: It's All in the Tumor. *Immunity*. 2019;50(6):1347-1349.

23. Barreira da Silva R, et al. Dipeptidylpeptidase 4 inhibition enhances lymphocyte trafficking, improving both naturally occurring tumor immunity and immunotherapy. *Nat Immunol*. 2015;16(8):850-8.

24. Liau NPD, et al. The molecular basis of JAK/STAT inhibition by SOCS1. *Nat Commun*. 2018;9(1):1558.

25. Ding Q, et al. CXCL9: evidence and contradictions for its role in tumor progression. *Cancer Med*. 2016;5(11):3246-3259.

26. Ho HH, Ivashkiv LB. Role of STAT3 in type I interferon responses. Negative regulation of STAT1-dependent inflammatory gene activation. *J Biol Chem*. 2006;281(20):14111-8.

27. Avalle L, et al. STAT1 and STAT3 in tumorigenesis: A matter of balance. *JAKSTAT*. 2012;1(2):65-72.

28. Marsolier J, et al. OncomiR addiction is generated by a miR-155 feedback loop in Theileria-transformed leukocytes. *PLoS Pathog*. 2013;9(4):e1003222.

29. Sharma N, et al. LILRB4 suppresses immunity in solid tumors and is a potential target for immunotherapy. *J Exp Med*. 2021;218(7): e20201811.

30. Francisco LM, et al. The PD-1 pathway in tolerance and autoimmunity. *Immunol Rev.* 2010;236:219-42.

31. Santos P, Almeida F. Role of Exosomal miRNAs and the Tumor Microenvironment in Drug Resistance. *Cells*. 2020;9(6):1450.

32. Tan S, et al. Exosomal miRNAs in tumor microenvironment. *J Exp Clin Cancer Res.* 2020;39(1):67.

33. Hamam R, et al. Circulating microRNAs in breast cancer: novel diagnostic and prognostic biomarkers. *Cell Death Dis*. 2017;8(9):e3045.

34. Cui M, et al. Circulating MicroRNAs in Cancer: Potential and Challenge. *Front Genet.* 2019;10:626.

35. Kong W, et al. Upregulation of miRNA-155 promotes tumour angiogenesis by targeting VHL and is associated with poor prognosis and triple-negative breast cancer. *Oncogene*. 2014;33(6):679-89.

36. Van Roosbroeck K, et al. Combining Anti-Mir-155 with Chemotherapy for the Treatment of Lung Cancers. *Clin Cancer Res*. 2017;23(11):2891-2904.

37. Kim JH, et al. Epstein-Barr virus latent membrane protein-1 protects B-cell lymphoma from rituximab-induced apoptosis through miR-155-mediated Akt activation and up-regulation of Mcl-1. *Leuk Lymphoma*. 2012;53(8):1586-91.

38. Croci DO, et al. Dynamic cross-talk between tumor and immune cells in orchestrating the immunosuppressive network at the tumor microenvironment. *Cancer Immunol Immunother.* 2007;56(11):1687-700.

39. Chen J, et al. Clinical significance of microRNA-155 expression in human breast cancer. *J Surg Oncol*. 2012;106(3):260-6.

40. Xiang X, et al. miR-155 promotes macroscopic tumor formation yet inhibits tumor dissemination from mammary fat pads to the lung by preventing EMT. *Oncogene*. 2011;30(31):3440-53.

41. House IG, et al. Macrophage-Derived CXCL9 and CXCL10 Are Required for Antitumor Immune Responses Following Immune Checkpoint Blockade. *Clin Cancer Res*. 2020;26(2):487-504.

42. Dangaj D, et al. Cooperation between Constitutive and Inducible Chemokines Enables T Cell Engraftment and Immune Attack in Solid Tumors. *Cancer Cell*. 2019;35(6):885-900 e10.

43. Ribas A. Adaptive Immune Resistance: How Cancer Protects from Immune Attack. *Cancer Discov*. 2015;5(9):915-9.

44. Lan H, et al. MicroRNAs as potential biomarkers in cancer: opportunities and challenges. *Biomed Res Int*. 2015:125094.

45. Yoshihara K, et al. Inferring tumour purity and stromal and immune cell admixture from expression data. *Nat Commun*. 2013;4:2612.

46. Cui X, et al. SCISSOR: a single-cell inferred site-specific omics resource for tumor microenvironment association study. *NAR Cancer*. 2021;3(3):zcab037.

47. Cancer Genome Atlas N. Comprehensive molecular portraits of human breast tumours. *Nature*. 2012;490(7418):61-70.

48. Lanczky A, et al. miRpower: a web-tool to validate survival-associated miRNAs utilizing expression data from 2178 breast cancer patients. *Breast Cancer Res Treat.* 2016;160(3):439-446.

49. Gyorffy B. Survival analysis across the entire transcriptome identifies biomarkers with the highest prognostic power in breast cancer. *Comput Struct Biotechnol J*. 2021;19:4101-4109.

50. Lanczky A, Gyorffy B. Web-Based Survival Analysis Tool Tailored for Medical Research (KMplot): Development and Implementation. *J Med Internet Res*. 2021;23(7):e27633.

51. Subramanian A, et al. Gene set enrichment analysis: a knowledge-based approach for interpreting genome-wide expression profiles. *Proc Natl Acad Sci U S A*. 2005;102(43):15545-50.

52. Janik K, et al. Efficient and simple approach to in vitro culture of primary epithelial cancer cells. *Biosci Rep.* 2016; 36(6):e00423

53. Wang J, et al. Tumor-derived adenosine promotes macrophage proliferation in human hepatocellular carcinoma. *J Hepatol.* 2021;74(3):627-637

Figures

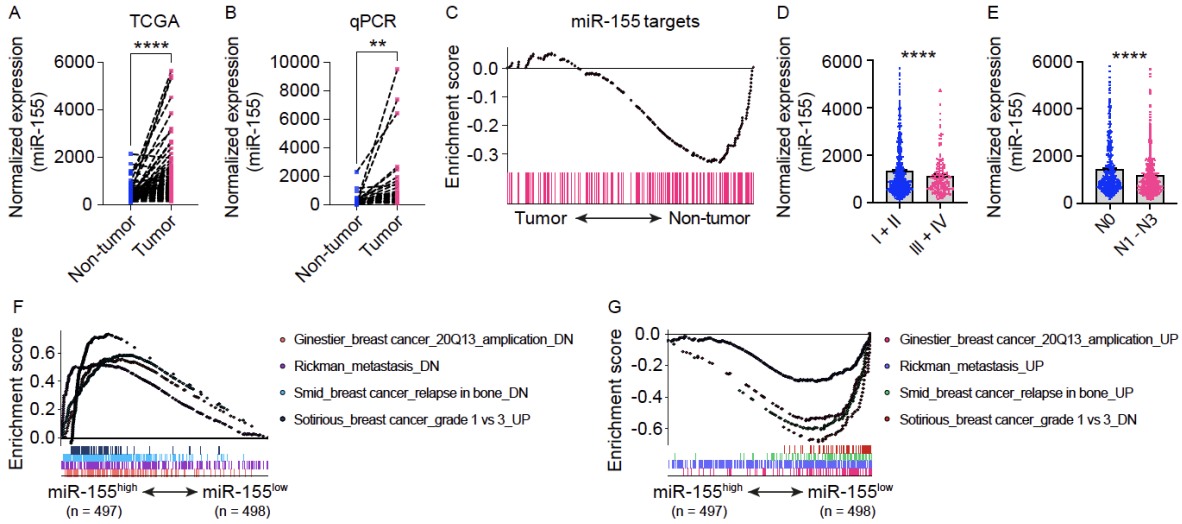

Figure 1. miR-155 expression levels in breast tumors are associated with disease progression. (**A**) Normalized miR-155 expression in paired human breast tumors and adjacent non-tumor tissues of TCGA data. n = 99. (**B**) Relative miR-155 level in paired human breast tumors and adjacent normal tissues by qPCR. n = 29. (**C**) GSEA analysis of TCGA data with respect to miR-155 target enrichment in tumor (n = 995) versus non-tumor (n = 99) area of human breast cancer patients. (**D**) Normalized miR-155 expression in breast tumors at different clinical stages. I + II, n = 732; III + IV, n = 204. (**E**) miR-155 levels in tumors of breast cancer patients with or without lymph node involvement. N0, n = 458; N1-3, n = 520. (**F**-**G**) Multi-GSEA analysis of tumor progression related gene signatures in miR-155^{high} versus miR-155^{low} tumors. The results are expressed as mean ± SEM. $^{**}P < 0.01$; $^{****}P < 0.0001$ by paired (**A**-**B**) or unpaired (**C**-**D**), two-tailed, Student's *t*-test. DN, down.

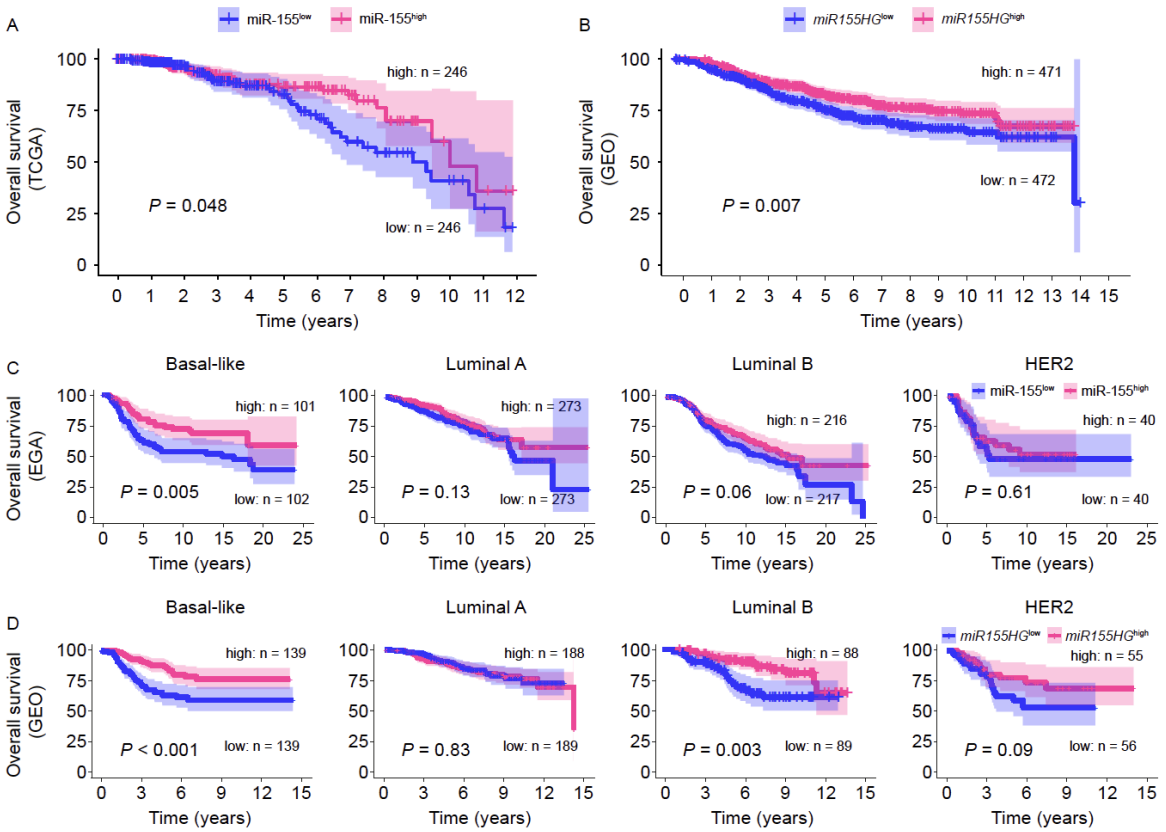

Figure 2. Higher miR-155 levels in human breast tumors are associated with better patient outcome. (**A**) Overall survival of breast cancer patients from TCGA database with high or low levels of miR-155 expression. Patients were divided into 2 groups according to the upper and lower quartiles of normalized miR-155 level in tumors. n = 246 in each group. (**B**) Overall survival of breast cancer patients from pooled GEO database with high and low levels of *miR155HG* expression. (**C-D**) Overall survival of breast cancer patients with different molecular classifications and miR-155 expression levels from EGA (**C**) and GEO (**D**) datasets. In **B**-**D**, the patients were divided into 2 groups according to the median value of miR-155 or *miR155HG* level in tumors. The curves comparison with the log-rank (Mantel-Cox) test revealed statistically significant differences as shown on graphs. HG, host gene; TCGA, The Cancer Genome Atlas; GEO, Gene Expression Omnibus; EGA, European Genome-Phenome Archive.

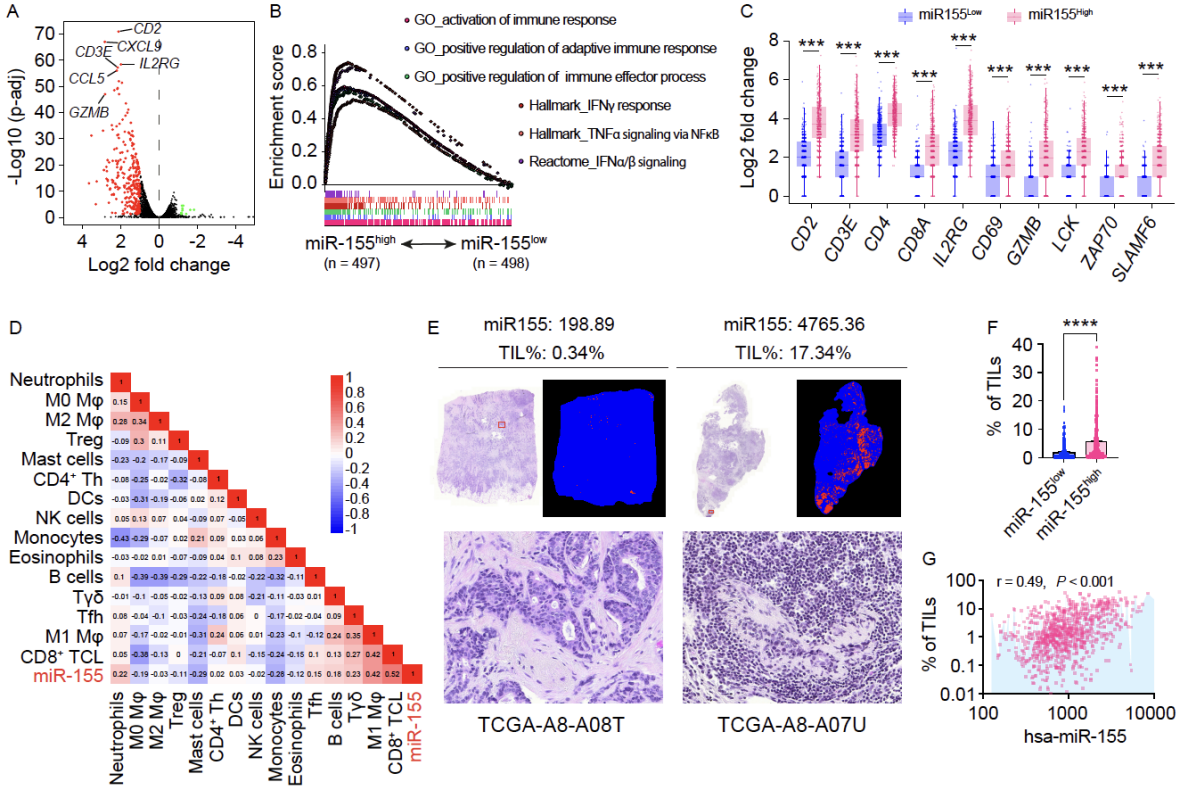

Figure 3. miR-155 expression levels in breast tumors are positively correlated with anti-tumor immunity. (**A**) Volcano plot for the differentially expressed genes between miR-155^{high} and miR-155^{low} tumors. (**B**) Multi-GSEA analysis of immune-related gene signatures in miR-155^{high} versus miR-155^{low} tumors. (**C**) Box plots comparing T cell-associated gene expression between miR-155^{high} (n = 497) and miR-155^{low} (n = 498) tumors. (**D**) Correlations of normalized miR-155 expression with predicted immune cell fractions in breast cancer tumors. n = 995. (**E**) The representative H&E staining and computational staining images of breast cancer tumors from TCGA, which were retrieved from CANCER Digital Slide Archive and TCIA, respectively. Normalized miR-155 expression and TILs percentage values are shown above corresponding images. (**F**) Quantification of estimated TILs proportions in miR-155^{high} and miR-155^{low} breast cancer tumors. n = 432 per group. (**G**) Correlations of miR-155 levels with the percentages of TILs in breast cancer tumor tissues. n = 864. (**C**) Wilcoxon rank sum test was carried out to compare the T cell activation related gene expression between miR-155^{high} and miR-155^{low} breast cancer tumors, ***$P < 0.001$. (**D** and **G**) P and r value were calculated based on the Pearson's correlation analysis. (**F**) Statistical significance was assessed using unpaired, two-tailed, Student's t-test and all data points are presented as mean ± SEM. ****$P < 0.0001$. TCIA, The Cancer Image Archive; TILs, tumor infiltrating lymphocytes.

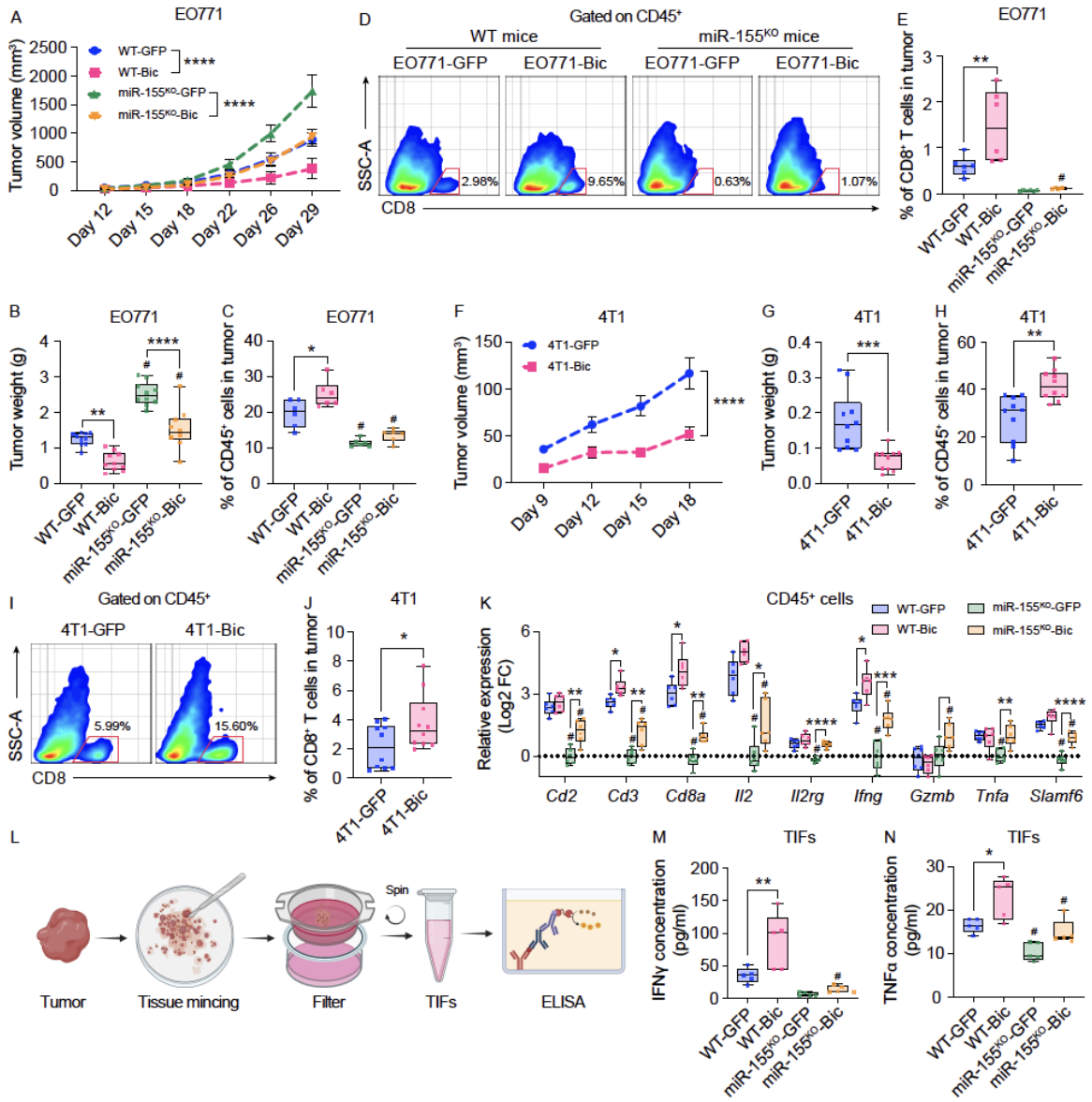

904

905 **Figure 4. Forced miR-155 overexpression inhibits tumor growth by increasing**
906 **immune cell influx.** (**A**) EO771-GFP and EO771-Bic tumor growth curves in WT or miR-
907 155^{KO} mice. n = 10-20 per group. (**B**) EO771 tumor weight 29 days post tumor inoculation.
908 n = 10 per group. (**C**) Frequencies of tumor infiltrating CD45^{+} leukocytes by flow cytometry.
909 n = 6 per group. (**D**) The representative pseudo color images from 6 samples of each group
910 showing the frequencies of CD8^{+} T cells gating from CD45^{+} cells; (**E**) quantified percentage
911 of CD8^{+} T cells in EO771 tumors. (**F**) 4T1-GFP and 4T1-Bic tumor growth curves in BALB/c
912 mice. 4T1 tumor weight (**G**) and CD45^{+} immune cell percentages (**H**) 19 days post tumor
913 inoculation. (**I**) The representative pseudo color images showing the frequencies of CD8^{+} T
914 cells gating from CD45^{+} cells; (**J**) quantified percentage of CD8^{+} T cells in 4T1 tumors. (**F-**
915 **J**), n = 10 per group. (**K**) T cell activation-related gene expression in sorted tumor infiltrating
916 CD45^{+} cells by qPCR. n = 6 per group. (**L**) Schematic image illustrating the procedure of
917 TIFs collection from tumor tissue and ELISA. IFNγ (**M**) and TNFα (**N**) protein concentrations
918 in tumor interstitial fluids (TIFs). Statistical analysis of (**A**) and (**F**) was performed using two-
919 way analysis of variance followed by Tukey test. Statistical significance was assessed using

two-tailed Student's *t* test for comparing 2 groups (**G**, **H** and **J**) and one-way ANOVA followed by Tukey's post-hoc test for multiple groups (**B**, **C**, **E**, **K**, **M** and **N**). All data points are presented as mean ± SEM. $^{\#}P < 0.05$ compared to WT counterparts; $^{*}P < 0.05$, $^{**}P < 0.01$, $^{***}P < 0.001$, $^{****}P < 0.0001$. TIFs: tumor interstitial fluids.

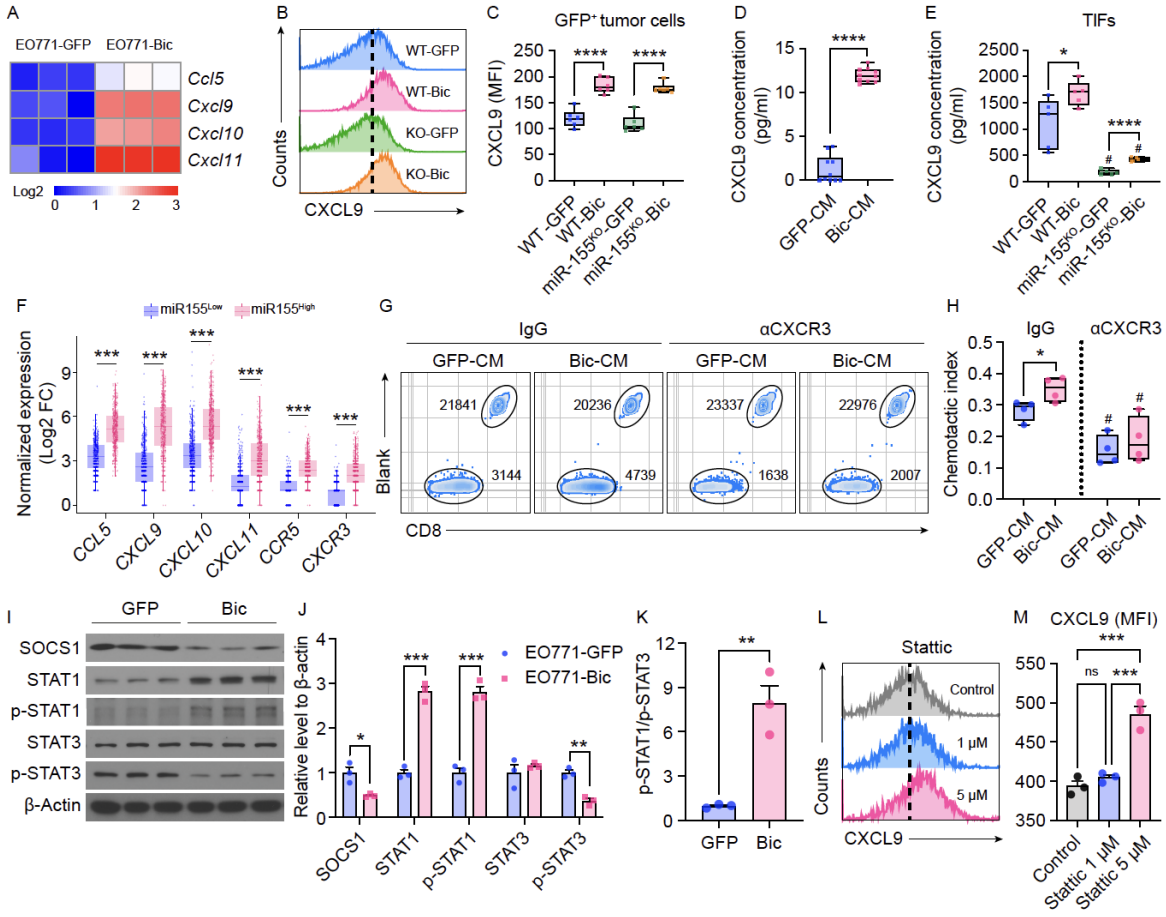

Figure 5. miR-155 overexpression enhances T cell recruitment by upregulating CCL5 and CXCL9/10/11 expression via tilting the pSTAT1/p-STAT3 ratio. (**A**) *Ccl5* and *Cxcl9/10/11* expression by qPCR. n = 3 per group. (**B and C**) Intracellular CXCL9 expression in EO771-GFP/Bic cells retrieved from tumor tissue (GFP^{+} cells) by flow cytometry, representative histograms (**B**) and quantified MFI of CXCL9 (**C**) are shown. n = 6 per group. CXCL9 concentration in cell culture media (**D**) and TIFs (**E**) by ELISA. n = 6 per group. (**F**) Expression of T cell recruitment related genes in miR-155^{high} (n = 497) and miR-155^{low} (n = 498) human breast cancer. (**G**) In vitro T cell migration towards EO771-GFP/Bic cell culture media, representative zebra plots showing the number of T cells and beads by flow cytometry. (**H**) The chemotactic index of (**G**) was calculated based on estimated cell numbers using counting beads. n = 4 per group. (**I**) Representative western blotting bands showing SOCS1, STAT1/STAT3 levels in EO771-GFP or EO771-Bic cells. (**J**) Blots of (**I**) was quantified relative to β-Actin expression. n = 3 per group. For samples run on different gels, separate loading controls were provided in Supplemental Unedited Western Blot images. (**K**) pSTAT1 to pSTAT3 ratio based on band intensity. n = 3 per group. (**L and M**) Intracellular CXCL9 expression in EO771 parental cells 24 hours post STAT3 inhibitor (Stattic) treatment; the representative histograms (**L**) and quantified MFI of CXCL9 (**M**) are shown. n = 3 per group. Statistical significance in all figures except (**F**) was assessed using the unpaired, two-tailed, Student's *t*-test; the statistic results shown in (**F**) were carried out by Wilcoxon rank sum test. All data points are presented as mean ± SEM. $^{\#}P < 0.05$ compared to WT counterparts; $^{*}P < 0.05$, $^{**}P < 0.01$, $^{***}P < 0.001$, $^{****}P < 0.0001$.

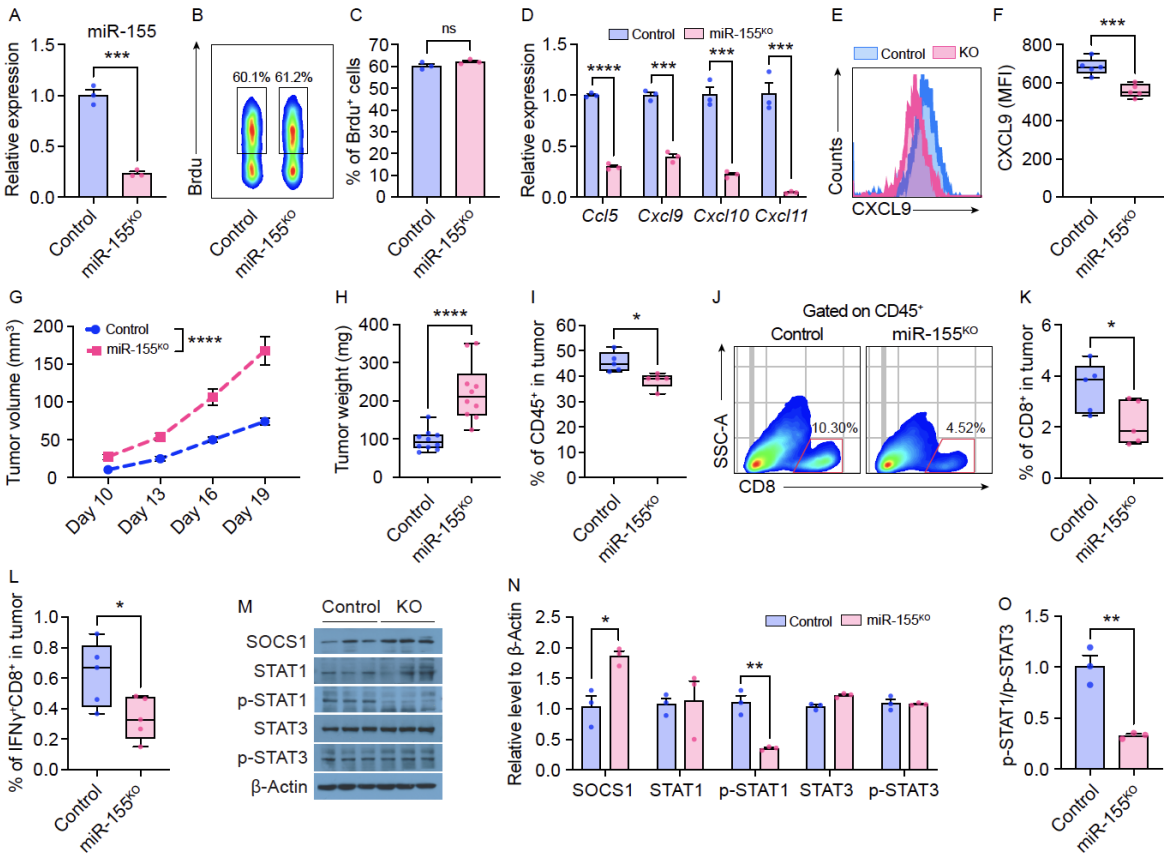

Figure 6. miR-155 knock out in EO771 cells promotes tumor growth by impairing anti-tumor immune infiltration. (**A**) Validation of miR-155 expression in miR-155^{KO} EO771 cells by qPCR. n = 3 per group. Representative pseudo color image (**B**) and quantified data (**C**) showing percentage of Brdu^{+} Control and miR-155^{KO} EO771 cells. n = 3 per group. (**D**) *Ccl5* and *Cxcl9/10/11* expression in Control and miR-155^{KO} EO771 cells by qPCR. n = 3 per group. Representative histograms (**E**) and quantified MFI (**F**) of Intracellular CXCL9 in Control and miR-155^{KO} EO771 cells by flow cytometry. n = 5 per group. (**G**) EO771-Control and EO771-miR-155^{KO} tumor growth curves in WT mice. n = 10 per group. (**H**) Tumor weight 19 days post tumor inoculation. n = 10 per group. (**I**) Frequencies of tumor infiltrating CD45^{+} leukocytes by flow cytometry. n = 5 per group. (**J**) The representative pseudo color images from 5 samples of each group showing the frequencies of CD8^{+} T cells gating from CD45^{+} cells; quantified percentage of CD8^{+} (**K**) and IFNγ^{+}CD8^{+} (**L**) T cells in tumors. (**M**) Representative western blotting bands showing SOCS1 protein, and STAT1/STAT3 protein and phosphorylation levels in EO771-Control or EO771-miR-155^{KO} cells. For samples run on different gels, separate loading controls were provided in Supplemental Unedited Western Blot images. (**N**) Blots of (**M**) was quantified relative to β-Actin expression. n = 3 per group. (**O**) The ratio of pSTAT1 to pSTAT3 in EO771-Control or EO771-miR-155^{KO} cells based on band intensity. n = 3 per group. Statistical significance in all figures was assessed using the unpaired, two-tailed, Student's *t*-test. All data points are presented as mean ± SEM. *$P < 0.05$, **$P < 0.01$, ***$P < 0.001$, ****$P < 0.0001$.

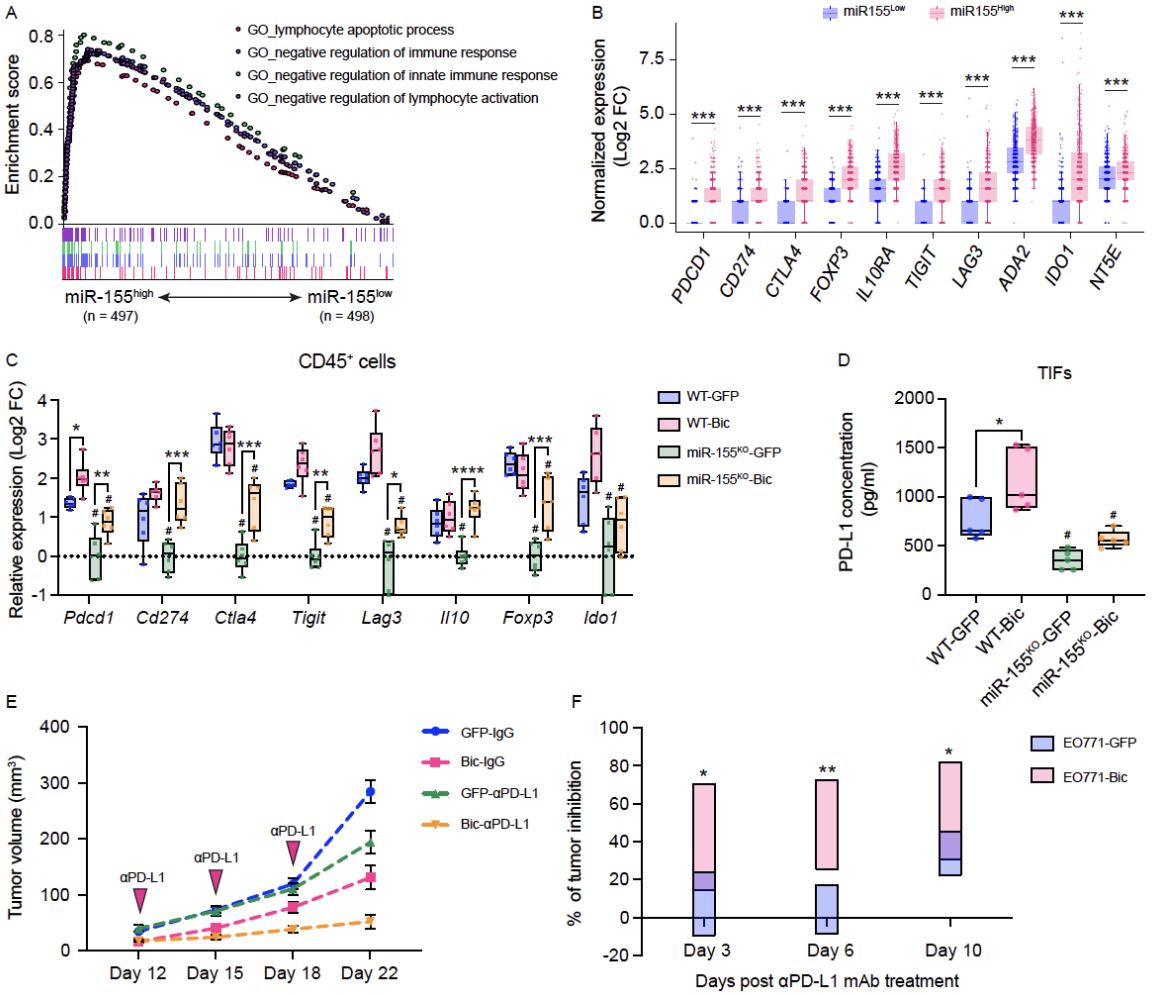

Figure 7. High miR-155 expression increases the level of immuno-break molecules and improves the tumor response to immunotherapy. (**A**) Multi-GSEA analysis showing the enrichment of negative immune response signatures in miR-155^{high} (n = 497) and miR-155^{low} (n = 498) human breast cancer tumors. (**B**) Box plot showing T cell exhaustive and immunosuppressive genes in miR-155^{high} (n = 497) and miR-155^{low} (n = 498) tumors. (**C**) Relative expression of T cell exhaustive and immunosuppressive genes in sorted tumor infiltrating leukocytes from tumor-bearing mice. n = 6 per group. (**D**) Soluble PD-L1 concentration in TILs by ELISA. n = 6 per group. (**E**) Tumor growth curves of EO771-GFP or EO771-Bic tumors of mice treated with anti-PD-L1 mAb, IgG2b was applied as isotype control. n = 7-10 per group. (**F**) Percent of tumor inhibition at various time points post anti-PD-L1 mAb treatment. n = 7-9 per group. Statistical significance was assessed using two-tailed Student's *t* test for comparing 2 groups (**F**) and one-way ANOVA followed by Tukey's post-hoc test for multiple groups (**C** and **D**). All data points are presented as mean ± SEM. $^{\#}P < 0.05$ compared to WT counterparts; $^{*}P < 0.05$, $^{**}P < 0.01$, $^{***}P < 0.001$.

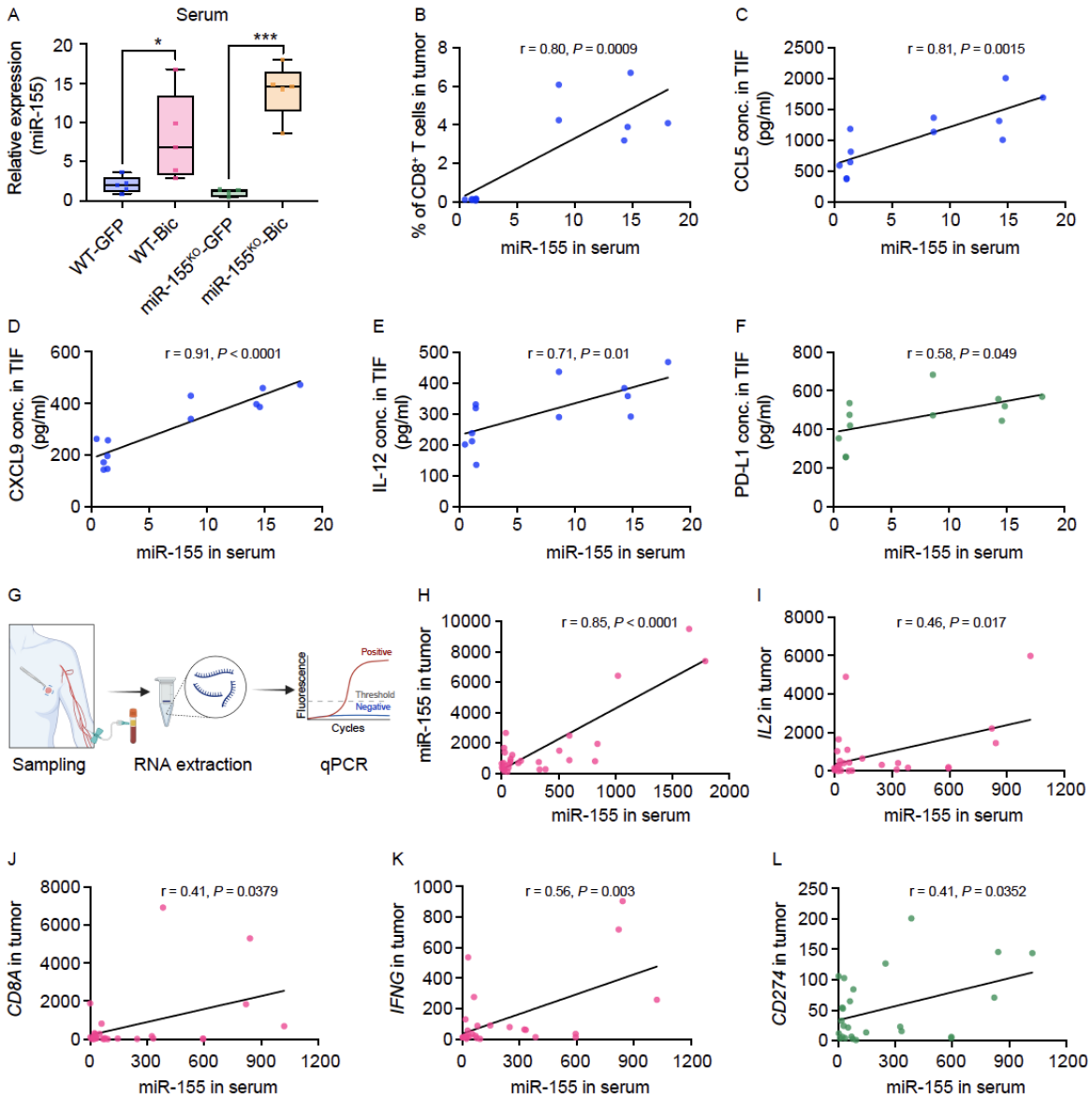

Figure 8. Circulating miR-155 mirrors anti-tumor immune status within breast tumors. (**A**) Relative miR-155 expression in serum collected from both WT and miR-155^{KO} mice carrying EO771-GFP or EO771-Bic tumors. n = 4 per group. Statistical significance was assessed using unpaired, two-tailed, Student's *t*-test and all data points are presented as mean ± SEM. **P* < 0.05, ****P* < 0.001. (**B**) The correlation between serum miR-155 levels measured by qPCR and the frequencies of CD8^{+} T cells in the tumors determined by flow cytometry. n = 12. (**C**-**F**) The correlation between serum miR-155 levels and CCL5 (**C**), CXCL9 (**D**), IL-12 (**E**), and soluble PD-L1 (**F**) concentrations in TIFs. n = 12. In a small cohort of human breast cancer samples, the expression of miR-155 and hallmark genes of T cell activation in serum, non-tumor, and tumor tissues were determined by qPCR. (**G**) Schematic image showing the procedure of sampling from breast cancer patients. (**H**) The correlation between serum miR-155 levels with tumor tissue miR-155 expression. n = 29. (**I**-**L**) The correlations between serum miR-155 levels and mRNA levels of *IL2* (**I**), *CD8A* (**J**), *IFNG* (**K**), and *CD274* (**L**) in human breast cancer tumor tissues. n = 26. *P* and r value in (**B**-**L**) were calculated based on the Pearson's correlation analysis.